Microphase Coexistence in Brushes

Leonid I. Klushin,† Tatiana M. Birshtein,* and Victor M. Amoskov

Institute of Macromolecular Compounds of the Russian Academy of Sciences, Bolshoi prospect 31, 199004, St. Petersburg, Russia

Received March 28, 2001; Revised Manuscript Received August 2, 2001

ABSTRACT: Computer modeling of solvent-immersed polymeric brushes with anisotropic attraction and polyelectrolyte brushes shows extended microphase coexistence; i.e., a collapsed microphase coexists with a swollen outer layer in a wide range of temperatures. We present an analytical theory that serves as a basis for understanding this phenomenon. The theory clarifies the nature of the first-order transition initiating the ordering and predicts the effect of the chain length, N, on the transition point and on the size of the critical nucleus of the ordered phase. For bidisperse brushes composed of chains of two fractions differing in contour length, the theory explains two mechanisms of ordering observed by self-consistent-field computer modeling and gives predictions for certain important features of the ordering (character of transitions, shifts of the transition points, and parameter domains of ordering mechanisms). Predictions of the analytical theory are in good agreement with the results of SCF computer modeling.

I. Introduction

Polymeric brushes are formed by long chains end-grafted to an impenetrable surface. Grafted polymer layers can be used for surface modification, for controlling the permeability of membranes, for regulating the particle interaction in colloids, etc. Natural realizations of brushes are also found in the elements of supramolecular architecture in di- and triblock copolymers under strong segregation conditions. From a theoretician's point of view brushes provide a model of a tethered, nonhomogeneous, self-organized structure. An attractive point of this model is that it can be explored in detail, the mathematics being lucid enough not to obscure its physical content. Some general results are obtained by simple scaling arguments, and a more detailed self-consistent-field theory is also available, including numerical schemes.

Phase transitions in polymeric brushes have been a topic of active research in the past decade. As far as planar brushes are concerned, it started with a discussion of whether such phase transitions exist at all.[1−3] Initial confusion was caused by the fact that a brush with isotropic interaction does not undergo an abrupt collapse with the decrease in the solvent quality but instead compactifies gradually, showing no signs of a phase transition. Soon after it was found that polyelectrolyte brushes as well as brushes with anisotropic interaction do exhibit phase transitions (providing grafting density is not too high).[4−17] The same was shown to be true for brushes with isotropic interaction characterized by anomalous behavior of higher virial coefficients (n-cluster model).[18,19]

For a simpler case of a bridging brush with chains attached to two surfaces, a complete analysis of phase segregation was performed.[8,11,12] It explained the smooth behavior of a brush with isotropic segment−segment attraction in terms of the critical point theory, a nondeformed brush at zero external pressure being similar to a supercritical fluid. For bridging bushes with anisotropic interaction between segments it was shown that the pressure at the critical point is positive, except for cases of dense grafting. Brushes with no external forces applied would display a typical first-order transition. Overall, bridging brushes are fundamentally similar to ordinary fluids as far as microphase segregation is concerned, the single major difference being that the critical pressure could be negative.

Brushes attached to just one surface are often described by the box model (due to Alexander and de Gennes) which, in fact, equates them to bridging brushes. However, from the point of view of phase coexistence, the fact that the free ends are distributed within the brush is of fundamental importance. Although some results obtained for the case of complete bridging remain valid, there are qualitatively new features as well. The most important difference is that brushes with distributed free ends display extended microphase coexistence: a collapsed microphase coexists with a swollen outer layer in a wide range of temperatures, in contrast to what one normally expects. This is what we are going to focus on in the present paper.

Extensive numerical calculations within the self-consistent-field approach were carried out for planar liquid-crystalline (LC)[13,14] and polyelectrolyte (PE) brushes[15−17] immersed in a solvent in the absence of external forces. As the governing parameter (reduced interaction strength in the LC and PE cases and also pH, degree of ionization, and ionic strength for PE brushes) is varied, one observes different phase states of the brush.

Results of numerical SCF calculations provide a common scenario of phase transitions in monodisperse LC and PE brushes.[13−17] The present paper aims to analyze and explain these results. All the discussion is focused on the LC transitions since the analytical theory is more transparent in this case. The theory we propose elucidates the nature of the unusual extended coexistence of microphases and describes the thickness of the emerging microphase at the transition point as well as the dependence of the transition point itself on the parameters of the brush. Analytical predictions for LC brushes are compared to the results of the numerical SCF calculations.

* To whom correspondence should be addressed.
† On leave from the American University of Beirut, Department of Physics, Beirut, Lebanon.

10.1021/ma0105338 CCC: $20.00
Published on Web 11/10/2001

Then, we extend the theory to describe in detail LC transitions and microphase coexistence in bidisperse brushes composed of chains of two different contour lengths. Numerical SCF calculations of bidisperse LC brushes have been carried out only very recently, demonstrating peculiar features absent in the monodisperse case.[20]

The paper is organized as follows:

First, we summarize the main results of the SCF calculations for monodisperse brushes. Then, we introduce a phenomenological theory as a basis for explaining extended phase coexistence, metastability, and other features observed in the computer modeling. In the next section, the theory is applied to the case of planar monodisperse brushes with anisotropic interaction in athermal solvent and compared to numerical results. The theory is then extended to explain the effects observed in the SCF modeling of bidisperse LC brushes. Applicability of the proposed approach to PE brushes and brushes collapsing via *n*-clusterization is discussed in the last section.

II. Monodisperse Brushes

A general picture that emerges from the SCF calculations for monodisperse planar brushes with PE or thermotropic LC interactions and immersed in a solvent can be summarized as follows:

1. At high or low values of the governing parameter (solvent quality χ for PE brushes and energy of anisotropic interaction η for LC brushes), a brush exists in a single-phase state: collapsed state or swollen state.

2. There is a whole range of intermediate values of the governing parameter where two microphases coexist within the same brush, their relative volumes gradually changing with the governing parameter. This is in contrast to a standard situation when phases can coexist only at a unique temperature once the pressure is fixed. In a planar geometry, the collapsed microphase is adjacent to the grafting plane, while the swollen microphase extends to the free surface of the brush. The brush chains fall into two categories: some reside entirely within the collapsed microphase, and others pass through it and form the swollen microphase. The free end distribution is bimodal.

3. The difference in the order parameter value in the two coexisting microphases is finite: in that sense, one is dealing with a typical first-order transition.

4. In the vicinity of the transition point metastable states, characteristic of a first-order transition, are observed. The equilibrium transition point defined from the crossing point of the two branches of the free energy depends on the polymerization index of the brush-forming chains, N.

5. At the transition point, the emerging ordered phase has a finite thickness which grows with N. However, if an appropriate thermodynamic limit $N \rightarrow \infty$ is taken, it comprises only a vanishing fraction of the total volume of the brush. Therefore, in the thermodynamic limit, the order parameter averaged over the whole brush does not exhibit a discontinuity at the transition point. By measuring the averaged order parameter, one would classify the transition as continuous.

The main features described above are illustrated by Figures 1−3. Figure 1 demonstrates the results of numerical SCF calculations (SCF modeling) for the density profile and the free end distribution for the case of PE brushes.[17] With the increase in the governing parameter χ the conventional PE brush (curve $\chi = 0$) first becomes microsegregated (curve $\chi = 1.9$) and eventually collapses completely (curve $\chi = 2.5$). The free ends distribution changes from a broad curve typical of a conventional swollen brush to a bimodal distribution and finally to a narrow peaked curve.

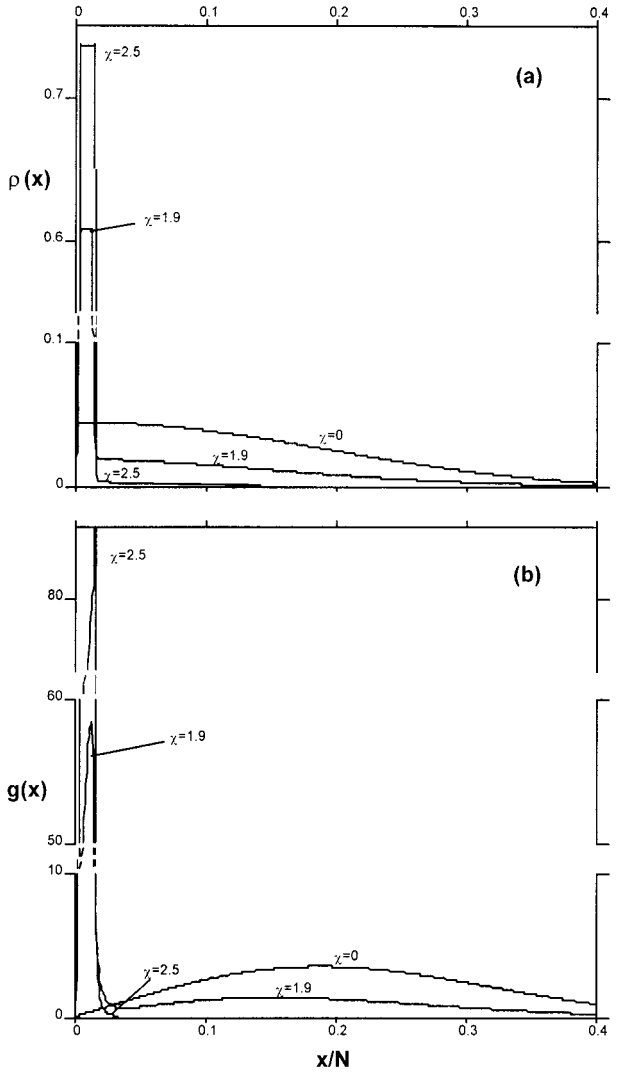

Figure 1. Density profiles $\rho(x)$ (a) and free ends distributions $g(x)$ (b) as obtained by SCF modeling for a PE brush for various χ (indicated in the figure); the surface grafting density $\sigma = 0.01$, the polymerization index $N = 500$, the degree of ionization $\alpha = 0.2$, and the ionic strength $\Phi_s = 10^{-5}$.

Results for a brush with anisotropic interaction at the transition point are displayed in Figure 2.[13,14] One can also clearly see two phases differing in the segment density and the bimodal shape of the free end distribution. Results for different values of the contour length parameter, N, at fixed surface grafting density σ are summarized by employing two scaling coordinates, x/N and $x/\sqrt{N}$, where x is the distance normal to the grafting plane. It is clear that the overall brush thickness scales as N while the results for the thickness of the emerging LC microphase at the equilibrium transition point (metastable states being excluded by a special procedure) seem to be consistent with the $N^{1/2}$ scaling. A similar scaling was obtained for PE brushes.[17]

Figure 3 displays the average density of a LC and PE brush in the equilibrium and metastable states as it changes with the corresponding governing parameter

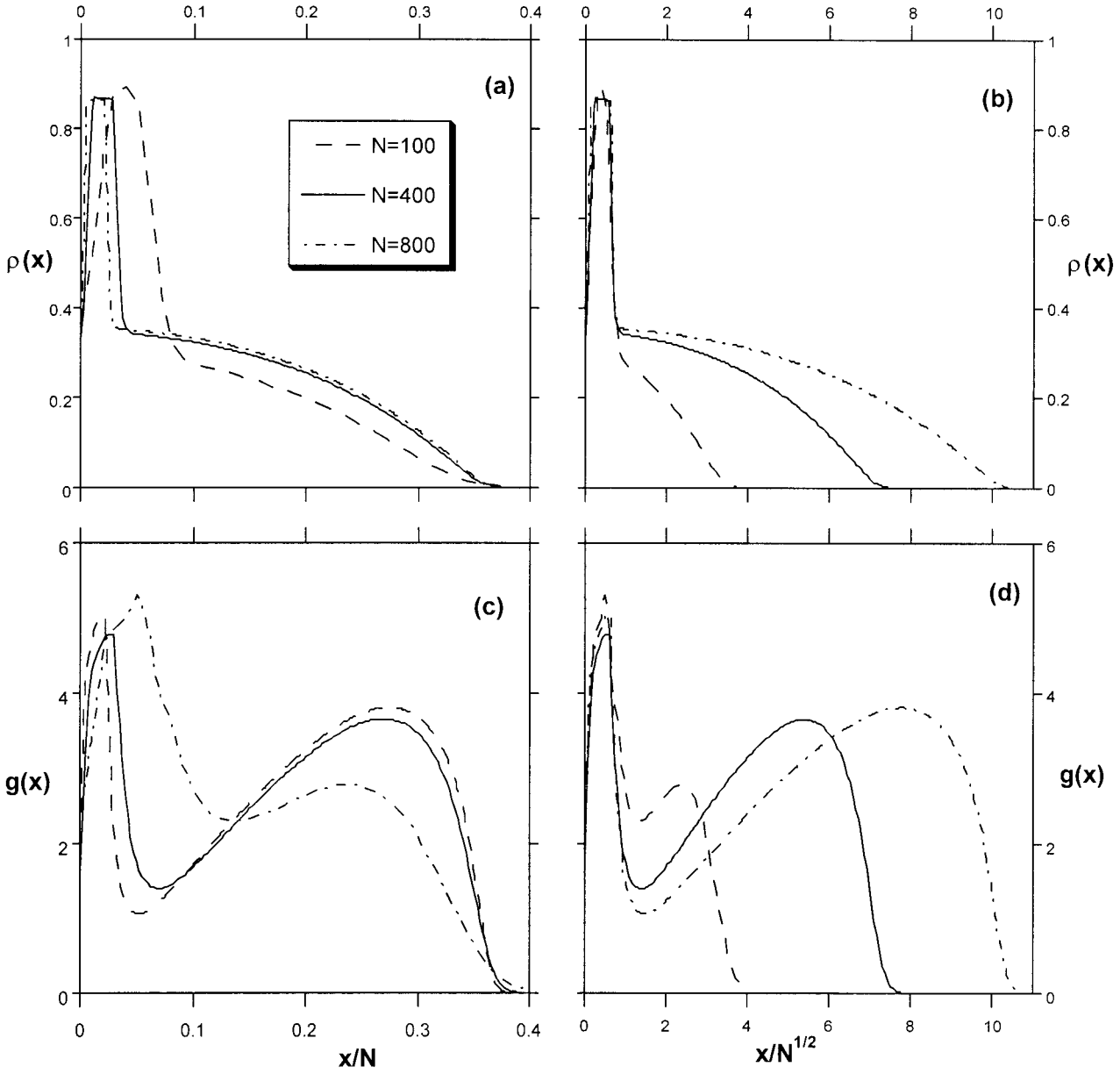

Figure 2. Density profiles $\rho(x)$ (a, b) and free ends distributions $g(x)$ (c, d) as obtained by SCF modeling for LC brushes with various N (indicated in the figures, in (c) dashed and dash-dotted curves should be interchanged) at the phase transition point ($\eta = \eta_t$). The distance is scaled as x/N in (a, c) and as $x/\sqrt{N}$ in (b, d). Everywhere $\sigma = 0.1$ and $\chi = 0$.

(η or χ). As mentioned above, the position of transition point is shifted to lower values for larger N. It is clear that the jump in the average density decreases with increasing N. The range of η or χ where metastable states exist also narrows down with N.

Phenomenology of Extended Phase Coexistence. We start by trying to fit the main qualitative results into the framework of the standard discussion of phase coexistence. The Gibbs free energy of a homogeneous phase has the form $G(M,P,T) = M\mu(P,T)$, where M is the number of particles and μ is the chemical potential coinciding with the free energy per particle. Considering the possibility of only two phases, the phase composition at equilibrium is determined by the condition that the total free energy be a minimum with respect to the number of particles in phase 2, M_2, the total number of particles, $M = M_1 + M_2$, being constant:

$$G = G_1(P,T,M_1) + G_2(P,T,M_2) = \min$$

In the standard case, G is a linear function of M_2: $G = M\mu_1 + M_2(\mu_2 - \mu_1)$. For $\mu_1 < \mu_2$, the minimum is attained at $M_2 = 0$; for $\mu_1 > \mu_2$ it is attained at $M_2 = M$ (see Figure 4a, lines T_1 and T_2 respectively). Phase coexistence is possible only along the coexistence line $T_t(P)$ defined by the equation $\mu_1(P,T) = \mu_2(P,T)$. At a fixed pressure P, there is a unique phase transition temperature $T_t(P)$ (Figure 4a, $T = T_t$). Relative volumes of the two coexisting phases are indeterminate at the transition point unless the conjugate variable, i.e., the total volume, is specified.

The picture is based on the assumptions that, within a given phase, the substance is homogeneous, and the Gibbs free energy is extensive in the number of particles. Then, the chemical potentials do not depend on the number of particles in a phase (apart from the interface effects that are usually incorporated separately). This is, of course, not universally correct. A system could be randomly chemically inhomogeneous,

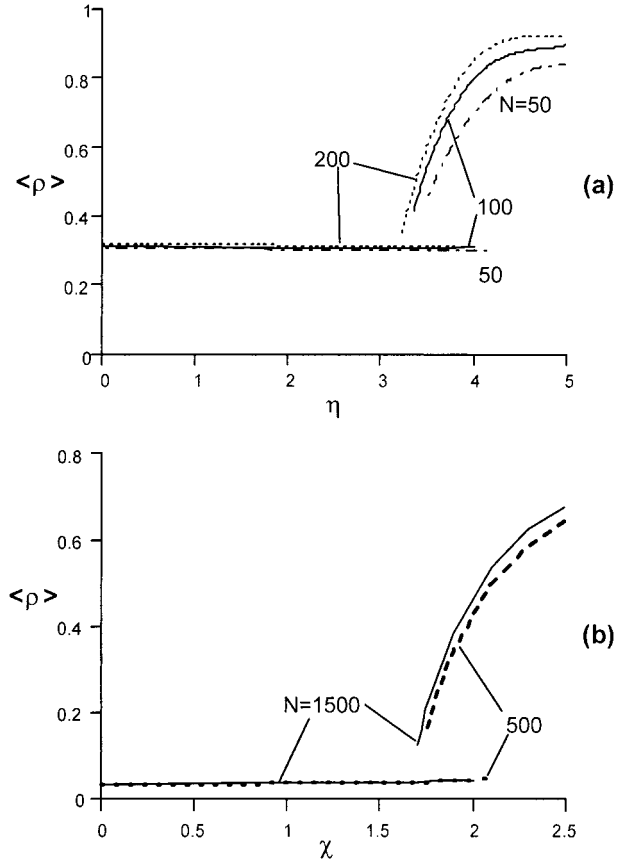

Figure 3. Results of the SCF modeling for the average segment density $\langle\rho\rangle$ in the brush vs the governing parameter of the transition (N is indicated in the figure): (a) LC brush with $\sigma = 0.1$ and $\chi = 0$; (b) PE brush with $\sigma = 0.01$, $\alpha = 0.2$, and $\Phi_s = 10^{-5}$.

which would lead to a finite temperature range of phase coexistence: a well-known example is given by DNA melting.

We will show that for polymeric brushes, even when they are chemically homogeneous, the chemical potential may explicitly depend on the size of the phase, and this provides a basis for explaining the numerical results discussed above. Note that when describing phase coexistence in a polymer system immersed in a solvent, it is more convenient to deal with the exchange (solvent−polymer unit) chemical potentials and the polymer osmotic pressure, rather than with the true chemical potentials and the total pressure.

To make the actual calculation more transparent, we start with a simple example without referring to any polymer specifics.

The dependence of chemical potentials on the number of particles means that $G = G_1(P,T,M-M_2) + G_2(P,T,M_2)$ becomes a nonlinear function of M_2. Two simple scenarios are obvious.

1. If $G(M_2)$ is a convex-up function (see Figure 4b), its minimum is always attained in a pure phase. The equilibrium transition point is defined by equating the free energies of two pure phases $G_1(M) = G_2(M)$. Formulation of this condition in terms of chemical potentials is not illuminating. Any phase coexistence in this case is thermodynamically unstable. Each pure phase is strongly metastable in the vicinity of the transition point. Within a realistic observation time, transitions would be observed only near the respective Curie points. An example of this behavior drawn from

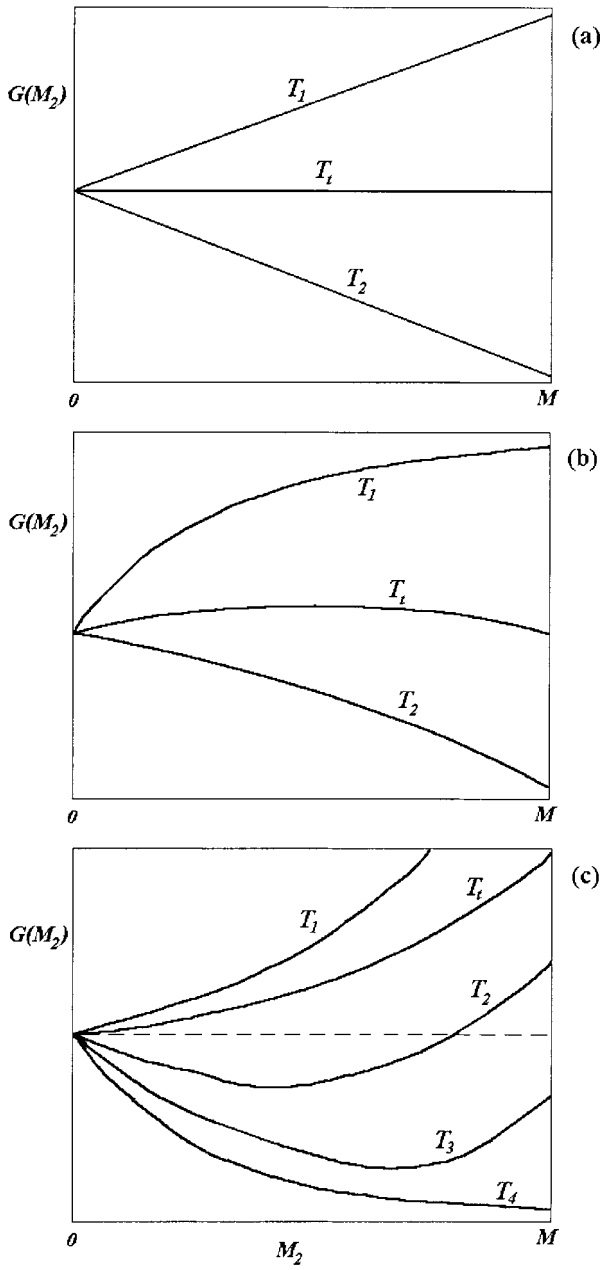

Figure 4. Schematic representation of the total free energy G as a function of the number of particles in the emerging phase M_2 for various temperatures T: (a) standard linear behavior; (b) convex-up; (c) convex-down. The chemical potential in the emerging phase μ_2 decreases for lower T; μ_1 is taken to be T-independent.

polymer science is given by a long flexible macromolecule undergoing a coil−stretch transition in an elongational flow.[21] This transition falls exactly under the scenario described, since the chemical potential of the stretched phase decreases with the number of segments making the free energy a convex-up function of the phase composition.

2. If $G(M_2)$ is a convex-down function (see Figure 4c), its minimum is attained in a phase-segregated system within a whole range of temperatures $T_t > T > T_4$. The convexity (down) of the free energy of a certain phase automatically means that its chemical potential is larger than the free energy per segment. This in turn implies that phase segregation always starts before one would expect a phase transition of the system "as a whole". The location of the minimum of $G(M_2)$ changes gradually

with temperature, and so does the phase composition determined by the equation $\mu_1(P,T,M-M_2)=\mu_2(P,T,M_2)$.

We will be interested in the case when the emerging (ordered) phase is "normal" in the sense that its chemical potential is a function of pressure and temperature only: $G_2 = M_2\mu_2$. The original disordered phase is, however, anomalous, so that G_1 is nonlinear in $M_1 = M - M_2$. The situation when the second phase is just emerging can be analyzed by expanding the free energy contributions in powers of the small parameter $x = M_2/M$:

$$G = G_1 + G_2 \cong G_1(M) + M\left((\mu_2 - \mu_1(M))x + \frac{1}{2}Bx^2\right) \quad (1)$$

Here $G_1(M)$ is the free energy of the pure disordered phase, and $\mu_1(M)$ is its chemical potential. Note that $G_1(M) \neq M\mu_1(M)$. For the planar geometry we are going to deal with the free energies of both phases should be taken per unit area. The quadratic term reflects the dependence of the chemical potential of the anomalous phase on the number of particles: $B = M[\partial^2 G_1(M)/\partial M_1{}^2] = M(\partial\mu_1/\partial M_1)|_{M_1=M}$. The convexity-down condition is satisfied if $B > 0$.

Minimizing with respect to x, one finds the minimum describing the equilibrium phase-segregated state, the fraction of particles in the emerging phase being

$$\bar{x} = \begin{cases} 0, & \text{if } \Delta\mu < 0 \\ \dfrac{\Delta\mu}{B}, & \text{if } \Delta\mu \geq 0 \end{cases} \quad (2)$$

with $\Delta\mu = \mu_1(M) - \mu_2$.

The size of the emerging phase grows with $\Delta\mu$ in a way similar to the order parameter behavior in a continuous phase transition.

The transition to a phase-segregated state occurs at $\mu_{2t} = \mu_1(M)$ when the free energy of the pure phase 2, $G_2(M)$, is still higher than $G_1(M)$; see curve T_t in Figure 4c.

3. Interfacial effects are easily incorporated in the last scenario. In the planar geometry, the interfacial energy per unit area, γ, has to be added to the free energy of phase-segregated states. It serves as a nucleation barrier separating the pure disordered phase from the phase-segregated system.

$$G(x) \cong G_1(M) + M\left((\mu_2 - \mu_1(M))x + \frac{1}{2}Bx^2\right) + \gamma, \quad x \in (0, 1) \quad (3)$$

The local minimum describing the phase-segregated state (eq 2) corresponds to true equilibrium only if it is lower than the free energy of the pure disordered phase: otherwise, it is only metastable. The equilibrium transition point is found from the condition $G_1(M) = G_1(M(1 - \bar{x})) + G_2(M\bar{x}) + \gamma$ to give

$$\mu_{2t} = \mu_1(M) - \Delta\mu_t \quad (4)$$

The transition point is shifted to lower values of μ_2 (lower temperature), the shift being M-dependent:

$$\Delta\mu_t = \left(\frac{2\gamma B}{M}\right)^{1/2} \quad (5)$$

At the equilibrium transition point, the number of particles in the emerging phase is also M-dependent:

$$M_{2t} = M\bar{x}_t = (2\gamma M/B)^{1/2} \quad (6)$$

Because of the nucleation barrier, one expects metastable states to exist in the vicinity of the transition point.

Application to Liquid-Crystalline Brushes. When applying the above scheme to brushes, we associate phase 1 with the swollen microphase and phase 2 with the collapsed liquid-crystalline microphase. The LC microphase is characterized by high density and is not influenced much by the polymeric nature of the brush. Numerical SCF calculations support the assumption we are going to use that the chemical potential of the collapsed LC microphase is a function of temperature only. For free nonconstrained brushes terminally attached to one planar surface, the osmotic pressure is fixed at zero value, $P = 0$, and there is no difference between the Gibbs and the Helmholtz free energies. Reduced interaction strength parameters are left as independent external variables.

The free energy of a swollen conventional brush (CB) per unit area is given by

$$G_{CB} = \frac{9}{10}\left(\frac{\pi v}{2}\right)^{2/3}\sigma^{5/3}N \quad (7)$$

where σ is the surface grafting density and v is the second virial coefficient of the segment−segment interaction ($v = 1$ in the athermal Flory−Huggins model).[22,23] Obviously, G_{CB} is not extensive in the total number of segments $M = \sigma N$. This anomalous property of the CB phase can be traced to a peculiar feature of tethered polymer systems: the osmotic pressure is fixed at zero value and does not depend on the segment concentration (importantly, translational degrees of freedom are suppressed). On the other hand, the free energy is a nonlinear function of concentration as one expects for an interacting system.

Defining the exchange chemical potential for a swollen brush requires a careful consideration. Generally speaking, the exchange chemical potential is a functional of both the starting contour length distribution density and the contour length distribution density specifying how exactly segments are added to or removed to another microphase in each chain. For a monodisperse brush, the starting distribution density is just $f(n) = \sigma\delta(n - N)$. The chemical potential can be reduced to an ordinary function only if one specifies a path in the functional space of contour length distribution densities. The path that actually governs phase coexistence is the one that has the steepest slope.

A closed expression for the chemical potential along an arbitrary path is not available, but two extreme cases illustrated by Figure 5 admit simple analytical treatment. If segments are removed from the CB phase uniformly (the same number of segments dN for each chain, the number of chains in the CB phase remaining fixed), then the contour length distribution density changes to $f = \sigma\delta(n - (N - \mathrm{d}N))$, and the chemical potential along this path is

$$\mu_{CB}^{(\text{uniform})} = \frac{1}{\sigma}\frac{\partial G_{CB}}{\partial N} = \frac{9}{10}\left(\frac{\pi v}{2}\right)^{2/3}\sigma^{2/3} \quad (8)$$

This chemical potential coincides with the free energy per segment, $G_{CB}/\sigma N$, and is constant along the path specified. If it were indeed the steepest slope of the free energy landscape, the phase coexistence would follow

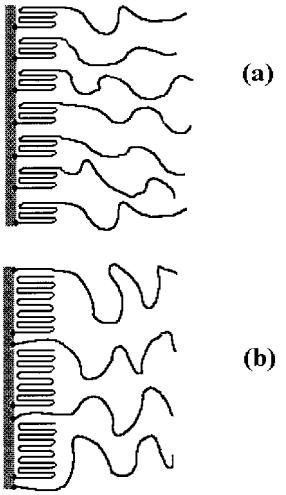

Figure 5. Illustration of the two paths for partial LC ordering in a swollen brush: (a) partial ordering of each chain in a uniform manner; (b) complete incorporation of a certain fraction of chains in the LC sublayer (other chains remain mostly in the outer swollen sublayer).

the standard picture illustrated by Figure 4a. Note that the path mentioned is the only one allowed in the "box model" or in a true bridging brush tethered to two parallel planes, where the LC phase transition always occurs at a certain temperature for the system as a whole.

Consider now the process when segments are transferred to another phase by removing entire chains. Then the distribution density changes to $f = (\sigma - d\sigma)\delta(n - N)$. The chemical potential along this path is

$$\mu_{CB} = \frac{1}{N}\frac{\partial G_{CB}}{\partial \sigma} = \frac{3}{2}\left(\frac{\pi\nu}{2}\right)^{2/3}\sigma^{2/3} \qquad (9)$$

It is clearly larger than the chemical potential for the uniform transfer of segments. There is strong evidence from the numerical SCF calculations and from the analytical theory of bidisperse brushes (discussed in the next section) that the second path indeed provides the steepest possible slope and hence governs the phase coexistence in brushes grafted to one surface only. Along this path the effective surface grafting density in the swollen phase is changing, and so does the chemical potential. The convexity-down condition is obviously satisfied: $(1/N)(\partial\mu_{CB}/\partial\sigma) = (1/N)(\pi\nu/2)^{2/3}\sigma^{-1/3} > 0$, and the coexistence scenario described above applies.

The LC microphase emerges when its chemical potential drops below μ_{CB} and is formed by some chains removed entirely from the swollen phase. It is exactly this possibility (absent in the bridging brush) that eventually leads to an extended temperature range of microphase coexistence in brushes.

A more accurate analysis takes into account the effects of chain deformation and the fact that, just because of the planar geometry, each chain has to contribute at least a small number of segments to the LC phase. Let ϵ be the fraction of chains belonging entirely to the LC layer. The other chains terminate within the CB phase: let α be the fraction of their segments within the LC layer. We take α as constant for all bridging chains. Both ϵ and α are small in the vicinity of the transition point.

The free energy of the CB microphase is $G_{CB}(\epsilon,\alpha) = (1 - \epsilon)^{5/3}(1 - \alpha)G_{CB}$ where G_{CB} is given by eq 7. We have employed the expression for the free energy of a swollen brush with the effective grafting density $(1 - \epsilon)\sigma$ composed of chains of length $(1 - \alpha)N$ and neglected the effects of the anisotropic interaction since the density of the CB microphase is typically much smaller than 1. The free energy per unit grafting area of the LC layer of thickness t can be written as

$$G_{LC} = t\rho_{LC}\mu_{LC} + G_{el} = t\rho_{LC}\mu_{LC} + \frac{3}{2}(1 - \epsilon)\sigma\frac{t^2}{\alpha N} + \epsilon\sigma\frac{\pi^2 N}{6t^2} \qquad (10)$$

where ρ_{LC} is the density of the LC phase, μ_{LC} is the bulk free energy of the LC phase per segment in the absence of deformation, and the last two terms account for the elastic deformation of chains within the LC layer. This deformation includes partial stretching of transit chains and normal compression of those chains that reside entirely within the LC layer. Numerical results suggest that the density within the LC layer is close to 1. Then

$$t \cong \epsilon\sigma N + (1 - \epsilon)\sigma\alpha N$$

Combining all the terms in the free energy of the microphase-segregated brush per unit grafting area gives

$$G(\epsilon,\alpha) = G_{CB}(1 - \epsilon)^{5/3}(1 - \alpha) + \sigma N\mu_{LC}(\alpha + \epsilon - \alpha\epsilon) + G_{el}(\epsilon,\alpha) + \gamma \qquad (11)$$

Minimizing with respect to α and ϵ, one obtains the following relationship in the vicinity of the transition point, where both α and ϵ are small:

$$\frac{\epsilon}{\alpha} = \left(\frac{3}{5}\left(\frac{\pi\nu}{2}\right)^{2/3}\sigma^{-4/3}\right)^{1/2} - 1 \sim \sigma^{-2/3} \qquad (12)$$

Equation 12 shows that if grafting is not too dense, $\sigma \ll 1$, then α is small compared to ϵ, and the LC layer is predominantly formed by segments of those chains that reside entirely within the LC phase. The bulk chemical potential of the LC layer is slightly shifted due to the elastic energy of the transit chains portions that reside in it. The local stretching is given by $t/\alpha N \cong \sigma(1 + \epsilon/\alpha) = (3/5)^{1/2}(\pi\nu/2)^{1/3}\sigma^{1/3}$, which is of the same order of magnitude as the stretching in the CB phase. Compression of chains in the LC layer turns out to be negligible, at least in the large N limit. The shift in the chemical potential per segment as compared to the LC phase without deformation is $\delta = \sigma(3/2)(t/\alpha N) \sim \sigma^{4/3}$ and does not depend on N. Taking this shift into account, one obtains up to leading terms in σ (for $\sigma \ll 1$):

$$G(\epsilon) \cong G_{CB} + N\sigma\left((\mu_{LC} + \delta - \mu_{CB})\epsilon + \frac{1}{2}\left(\frac{\pi\nu}{2}\right)^{2/3}\sigma^{2/3}\epsilon^2\right) + \gamma \qquad (13)$$

This form of the free energy is completely equivalent to eq 3 analyzed above. The equilibrium transition point follows from eq 4:

$$\tilde{\mu}_{LC} = \mu_{CB}(\sigma) - \Delta\mu_t(\sigma,N) \qquad (14)$$

where $\tilde{\mu}_{LC} = \mu_{LC} + \delta(\sigma)$ is the chemical potential of the LC phase including the elastic contribution of the transit chains, and the dependence on N and σ is shown explicitly. The N-dependent part of the shift is given

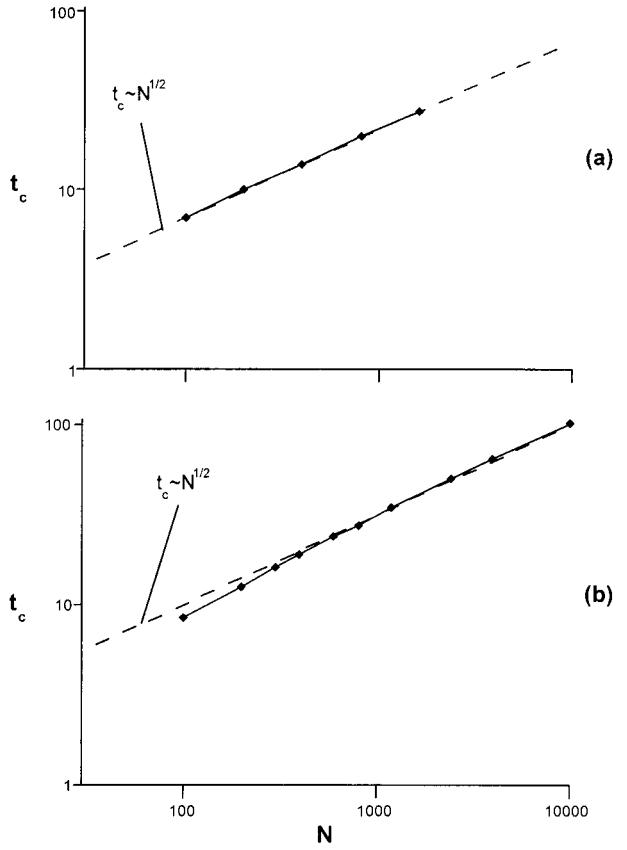

Figure 6. A log−log plot of the thickness of the critical LC nucleus vs N: (a) results of the SCF computer modeling; (b) results of the numerical analysis of eq 11; $\sigma = 0.1$ for both (a) and (b); straight lines represent the expected asymptotic behavior $t_c \sim N^{1/2}$.

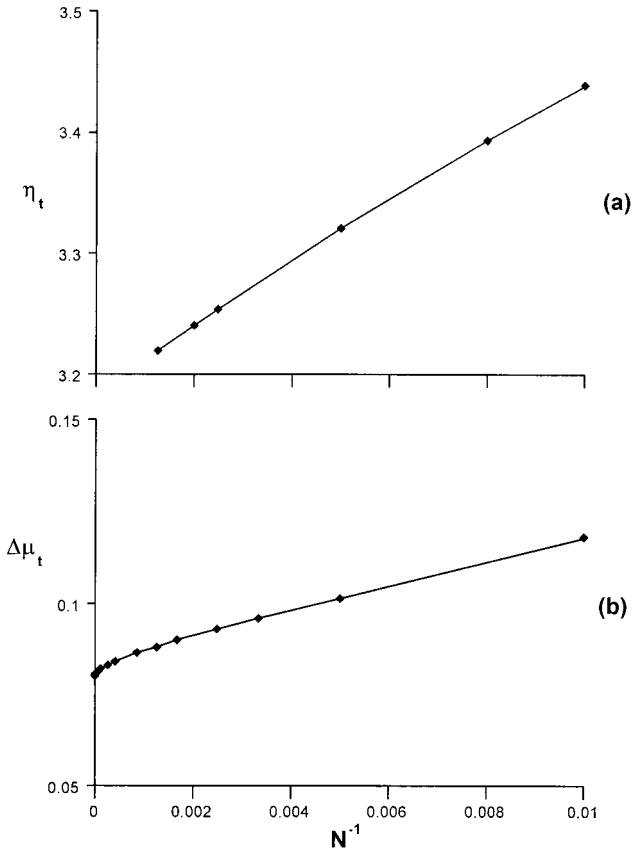

Figure 7. Chain length dependence of the transition point: (a) the transition value of the anisotropic interaction parameter, $\eta_t(N)$, vs $1/N$ obtained by the SCF computer modeling; (b) the chemical potential difference at the transition point, $\Delta\mu_t(N)$, vs $1/N$ obtained by numerical analysis of eq 11; $\sigma = 0.1$ for both (a) and (b).

by eq 5 with proper substitutions $M = N\sigma$ and $B = (\pi\nu/2)^{2/3}\sigma^{2/3}$:

$$\Delta\mu_t = (\pi\nu)^{1/3}(\sigma/2)^{-1/6}\gamma^{1/2}N^{-1/2} \tag{15}$$

The thickness of the LC layer at the equilibrium transition point is consistent with eq 6:

$$t_c = 2^{5/6}(\pi\nu)^{-1/3}\gamma^{1/2}\sigma^{1/6}N^{1/2} \tag{16}$$

In the $N \to \infty$ limit, $\Delta\mu_c \to 0$ and the transition occurs at $\mu_{\mathrm{LC}t}(\infty) = \mu_{\mathrm{CB}} - \delta$, so that eq 14 can be rewritten as

$$\mu_{\mathrm{LC}t}(N) = \mu_{\mathrm{LC}t}(\infty) - \Delta\mu_t(N) \tag{17}$$

In the model we are discussing, anisotropic interactions are introduced through the term $-{}^1/_2\eta s^2\rho^2$ in the free energy per unit volume, where η is the reduced anisotropic interaction parameter, s is the nematic order parameter, and ρ is the segment density ($\rho = 1$ for dense packing). This leads to a term $-\eta s^2\rho$ in the chemical potential of the LC phase. Since the parameters s and ρ in the LC phase change only little in the vicinity of the transition point (both are reasonably close to 1), μ_{LC} is well approximated by a linear function of η in this region. In terms of η, eqs 15 and 17 give for finite N

$$\eta_t(N) = \eta_t(\infty) + \Delta\eta_t(N) = \eta_t(\infty) + AN^{-1/2} \tag{18}$$

where A is independent of N.

Comparison to SCF Results. Results of the SCF computer modeling show that the predicted $N^{1/2}$ asymptotic scaling for the thickness of the critical LC nucleus is very well satisfied in the range $N = 100-1600$ (Figure 6a). In our analytical theory, there appear some corrections to scaling clearly visible up to about $N \sim 10^3$ (see Figure 6b). The points were obtained by direct numerical minimization of the free energy given by eq 11 for $\sigma = 0.1$ and $\gamma = 0.1$. We do not know the actual value of the surface tension in the lattice SCF model, but the overall shape of the curve in Figure 6b is fairly insensitive to it. Specifically, in the range of N explored by the SCF modeling, corrections to the true asymptotic $N^{1/2}$ behavior turn out to be within about 15% accuracy.

The main motivation for exploring corrections to scaling came from the SCF modeling results for the N-dependence of the shift in the transition point, displayed in Figure 7a. The data seem to suggest that

$$\Delta\eta_t(N) = \eta_t(N) - \eta_t(\infty) \sim N^{-1} \tag{19}$$

in contrast to the $N^{-1/2}$ scaling of eq 18. We believe that the chain lengths used in the SCF calculations are simply not large enough to display the $N^{-1/2}$ asymptotics. Figure 7b shows the chemical potential difference at the transition point, $\Delta\mu_t(N)$, vs $1/N$ obtained directly by minimization of the free energy given by eq 11 for $\sigma = 0.1$ and $\gamma = 0.1$. The points fall nicely on a straight line up to $N \sim 1000$, and only for $N > 2000$ is the $N^{-1/2}$ dependence clearly manifested.

Note that to obtain our simple analytical results, we had to assume that the fraction of chains forming the LC sublayer, ϵ, is very small. On the other hand, the

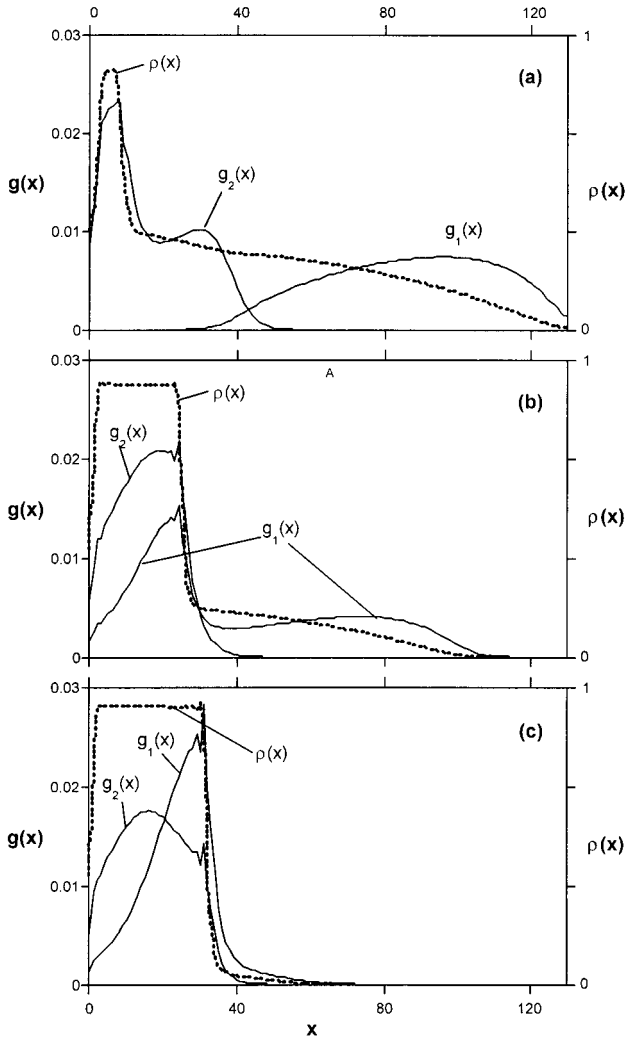

Figure 8. Total density profile $\rho(x)$ and partial free ends distributions $g_1(x)$, $g_2(x)$ for long and short fractions, respectively, illustrating the two-stage LC ordering in a bidisperse brush with the increase in the interaction parameter η: (a) the first transition point; (b) just over the second (continuous) transition; (c) complete LC ordering; $N_1 = 400$, $N_2 = 200$; $\sigma_1 = 0.05$, $\sigma_2 = 0.05$.

thickness of this sublayer is found to be of order $N^{1/2}$. This imposes a rather stringent condition $N\sigma\epsilon \sim N^{1/2}$ or $N \sim (\epsilon\sigma)^{-2}$. Taking $\sigma = 0.1$ and $\epsilon = 0.3$, one can see that $N \sim 10^3$ is a reasonable estimate for the crossover value.

We conclude that is natural to expect considerable corrections to scaling up to $N \sim 10^3$. The fact that the thickness of the critical nucleus in the SCF modeling follows the $N^{1/2}$ law down to $N = 100$ may be due to some cancellation effects. In particular, the actual values of the LC sublayer density and of the surface tension coefficient may vary slightly with N, which is not accounted for in the analytical theory.

III. Bidisperse LC Brushes

Very recently, numerical SCF results were obtained for planar LC brushes composed of two types of chains differing only in their contour length, $N_1 > N_2$, and grafted at surface densities σ_1 and σ_2, respectively.[20] Note that in the present section subscripts 1 and 2 refer to chains of different length in one and the same brush (in contrast to the subsection on phenomenology of extended phase coexistence where these subscripts

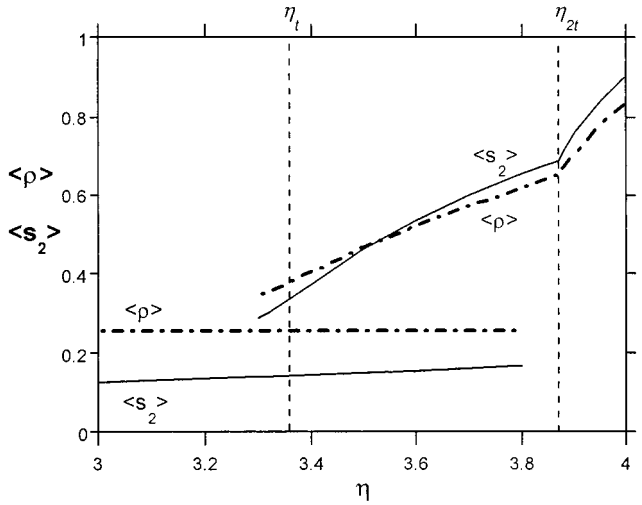

Figure 9. Average segment density and average order parameter in a bidisperse brush vs the interaction parameter η; $N_1 = 800$, $N_2 = 200$; $\sigma_1 = 0.01$, $\sigma_2 = 0.09$.

referred to two different phases). Some special features include the dependence of the transition point on the relative composition and the possibility of a two-stage LC ordering. In the following, we discuss only the case when the two components differ in their contour length considerably ($\Delta N = N_1 - N_2$ is at least of the same order as the shorter chain length $\Delta N \sim N_2$) when the analytical SCF theory describing bidisperse brushes is well justified.[24,25]

A Summary of the SCF Modeling Results. *Two-Stage Ordering.* For the case when the fraction of longer chains is not too high, numerical SCF calculations show that liquid-crystalline ordering proceeds with the decrease in temperature in two stages as illustrated by Figure 8. The first stage is dominated by shorter chains (Figure 8a) and follows very closely the transition in a reference monodisperse brush consisting of short N_2 chains at the same total grafting density $\sigma = \sigma_1 + \sigma_2$. (For brevity, we shall refer to this as (N_2, σ) brush.) In other words, the fact that some chains in a bidisperse brush are actually longer is of no consequence at this stage. The LC sublayer is formed by short chains only. The emergence of this sublayer (at the transition point $\eta = \eta_t$) is accompanied by a jump in the average density and in the average order parameter (see Figure 9), the same way it happens for a monodisperse brush. The jump is due to the nucleation barrier associated with creating a planar interface. The transition point coincides with that in a monodisperse (N_2, σ) brush.

At lower temperatures (larger anisotropic interaction parameters η) all the shorter chains are eventually absorbed in the LC phase, and at some point $\eta = \eta_{2t}$ the average density shows a discontinuity in the slope rather than a jump (see Figure 9). This marks the onset of the second stage when longer chains start collapsing onto the LC sublayer (Figure 8b) and has the features of a typical continuous (second-order) phase transition. The position of the second transition point is primarily affected by the grafting density of long chains, σ_1. The slope of the curve in the vicinity of the transition point changes very little with the brush parameters (see Figure 10).

Mixed One-Stage Mechanism. If the fraction of shorter chains $\sigma_2/(\sigma_1 + \sigma_2)$ is small enough, LC ordering proceeds in one stage, and the critical nucleus is formed by chains of both types (see Figure 11 at $\eta = \eta_t$). The

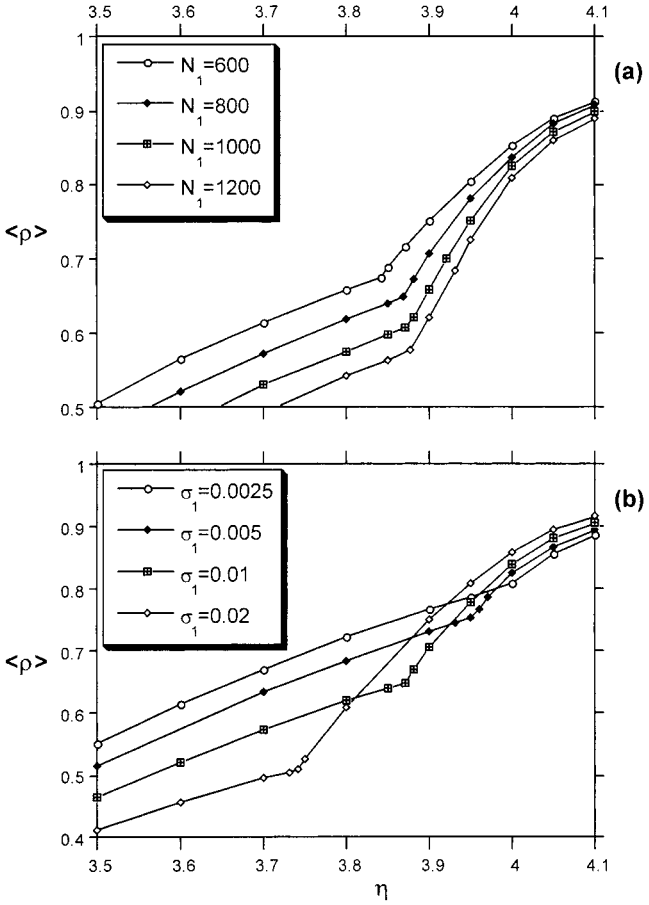

Figure 10. Average segment density in a bidisperse brush in the vicinity of the second (continuous) transition: (a) effects of the chain length of the long fraction (indicated in the figure) for $N_2 = 200$; $\sigma_1 = 0.01$, $\sigma_2 = 0.09$; (b) effect of the partial grafting density: σ_1 indicated in the figure, the total grafting density is fixed at $\sigma = 0.1$ for $N_1 = 800$, $N_2 = 200$.

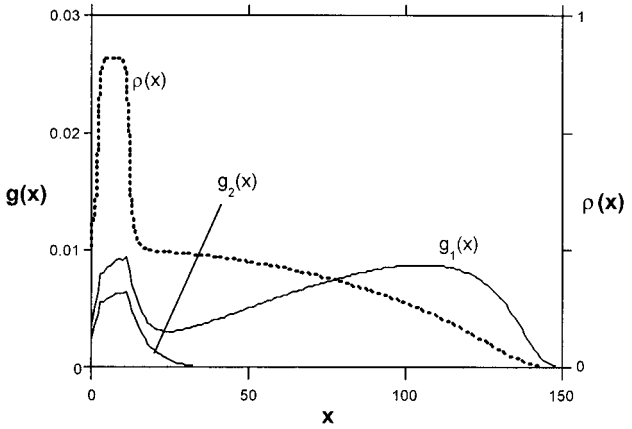

Figure 11. Total density profile $\rho(x)$ and partial free ends distributions $g_1(x)$, $g_2(x)$ for long and short fractions, respectively, illustrating the formation of the critical LC nucleus in a bidisperse brush by the one-stage ordering mechanism; $N_1 = 400$, $N_2 = 200$; $\sigma_1 = 0.09$, $\sigma_2 = 0.01$; $\eta = \eta_t = 2.282$.

transitionpoint is somewhere between the two values for the reference monodisperse (N_1, σ) and (N_2, σ) brushes (see Figure 12). The mixed mechanism is operating when the fraction of shorter chains is smaller than a certain value, $\{\sigma_2^*\}/\{\sigma\}$. This characteristic value is independent of N_1 for sufficiently large values of N_1.

Analytical Theory. A natural extension of the approach presented above allows us to explain the

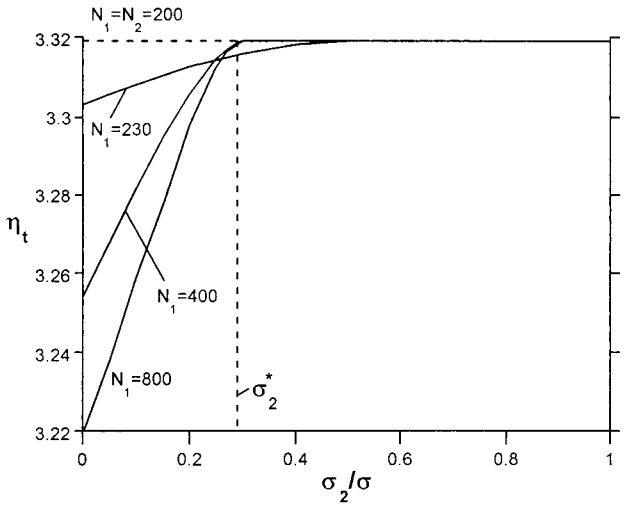

Figure 12. Effect of the relative partial grafting density σ_2/σ on the first transition point in a bidisperse brush: the short fraction length is fixed at $N_2 = 200$; the long fraction chain length is indicated in the figure; $\sigma = 0.1$.

existence of the two mechanisms, their main features, and domains of existence. We can verify some scaling predictions against the SCF modeling results, although quantitative comparison is sometimes difficult. The validity of the expansion we are going to employ imposes even stronger conditions on N_1 and N_2 than in the case of a monodisperse brush.

The analytical SCF theory of bidisperse brushes with isotropic interaction provides expressions for the chemical potentials associated with removing a short or a long chain from the CB phase.[24,25] As in the monodisperse case, these are the relevant chemical potentials determining the microphase coexistence. For short chains

$$\mu_2 = \frac{3}{2}\left(\frac{\pi\nu}{2}\right)^{2/3}\sigma^{2/3} \tag{20}$$

which is exactly the same as in a monodisperse brush, while for longer chains

$$\mu_1 = \frac{3}{2}\left(\frac{\pi\nu}{2}\right)^{2/3}(\sigma^{2/3}q + {\sigma_1}^{2/3}(1 - q)) \tag{21}$$

where $q = N_2/N_1 < 1$. It is clear that since $\sigma_1 < \sigma$, μ_1 is always lower than μ_2. To simplify the notation of this section, we will be dropping the subscript CB when referring to chemical potentials of the swollen brush.

Equation 13 is to be replaced by an expansion of the free energy in powers of two variables, ϵ_1 and ϵ_2 for the longer and shorter chains, respectively. The resultant quadratic form is

$$G = G_0 + (\tilde{\mu}_{LC} - \mu_1)N_1\epsilon_1 + (\tilde{\mu}_{LC} - \mu_2)N_2\epsilon_2 + \frac{1}{3\sigma}\mu_2 N_2\left(\left(1 + \frac{\Delta N}{N_2}\frac{\sigma^{1/3}}{{\sigma_1}^{1/3}}\right){\epsilon_1}^2 + 2\epsilon_1\epsilon_2 + {\epsilon_2}^2\right) + \gamma \tag{22}$$

where $\tilde{\mu}_{LC}$ includes the elastic contribution from the stretched portions of the transit chains within the LC sublayer (see eq 14).

Two-Stage Ordering: The First Stage. To characterize the emerging microphase-segregated state, we have to minimize G in the positive quadrant of the (ϵ_1 − ϵ_2) plane. At high temperatures ($\tilde{\mu}_{LC} > \mu_2 > \mu_1$) the constrained minimum is attained at the origin $\epsilon_1 = \epsilon_2$

= 0. A nontrivial minimum appears when $\tilde{\mu}_{LC}$ drops below μ_2. In the range $\mu_2 > \tilde{\mu}_{LC} > \mu_1$ the minimum is constrained to the ϵ_2 axis ($\epsilon_2 = 0$), so that the problem reduces identically to that of a monodisperse (N_2, σ) brush. If a deep enough minimum is achieved while still on the ϵ_2 axis, the transition to the microphase-segregated state involves only short chains. The critical nucleus is composed entirely of the shorter chains, and the transition point is the same as in the (N_2, σ) brush.

To understand what happens with further lowering of the chemical potential of the LC state beyond the validity range of expansion (22), we go back to general expressions (20, 21) for the chemical potentials as functions of the varying grafting densities σ_1 and σ_2. As shorter chains are removed from the swollen phase, the effective grafting density of shorter chains in the swollen phase σ_2 decreases while σ_1 remains constant. Hence, both μ_1 and μ_2 decrease, but importantly, μ_2 always remains higher than μ_1. At a given temperature, the effective σ_2 characterizing the short chain content in the outer sublayer is determined by equation $\mu_2(\sigma_1 + \sigma_2^{(eff)}) = \tilde{\mu}_{LC}(\eta)$ This goes on until all the shorter chains are incorporated in the LC sublayer, in agreement with the results of the SCF computer modeling.

Two-Stage Ordering: The Second Stage. At some temperature, the effective σ_2 vanishes and so does the difference between μ_1 and μ_2. Below that temperature long chains start collapsing onto the LC sublayer. The start of this process manifests itself as a discontinuity in the slope of the average density curve vs η. Hence, the point of the second transition is determined by the following simple equation

$$\tilde{\mu}_{LC} = \frac{3}{2}\left(\frac{\pi\nu}{2}\right)^{2/3}\sigma_1^{2/3} \qquad (23)$$

where the right-hand side is the chemical potential in the outer sublayer formed by the tails of longer chains. Neglecting the elastic contribution to $\tilde{\mu}_{LC}$ (which is of higher order in σ), we immediately find that the point of the second (continuous) transition should essentially depend only on the grafting density of longer chains. The larger the grafting density, the smaller is η at the transition, the shift being proportional to $\sigma_1^{2/3}$. Results of the SCF calculations support this prediction very nicely, as illustrated by Figure 13. In contrast to the first jumpwise transition (associated with creating a critical nucleus), the second transition occurs when the interface already exists. Hence, the transition is continuous, and its position is predicted to be independent of the contour length of longer chains. This is consistent with results of the SCF modeling for large enough N_1 (see Figure 10a).

To the leading order, the number of segments in the LC sublayer grows linearly with the chemical potential shift of the LC phase, as seen from eq 2. The number of segments joining the LC phase due to the long chain removal can be written as

$$dM = B^{-1}d\mu_{LC} = \left(\frac{\pi\nu}{2}\right)^{-2/3}(\tilde{N}_1\sigma_1^{1/3})\, d\mu_{LC} \qquad (24)$$

where $\tilde{N}_1$ is the contour length of the longer chain tails that form the outer CB layer. It is clear that the slope $dM/d\mu_{LC}$ is proportional to the thickness of the outer CB layer (taken at the point of the second transition). Recalculating this in terms of the slope of the average density vs η, we obtain a simple expression in the limit

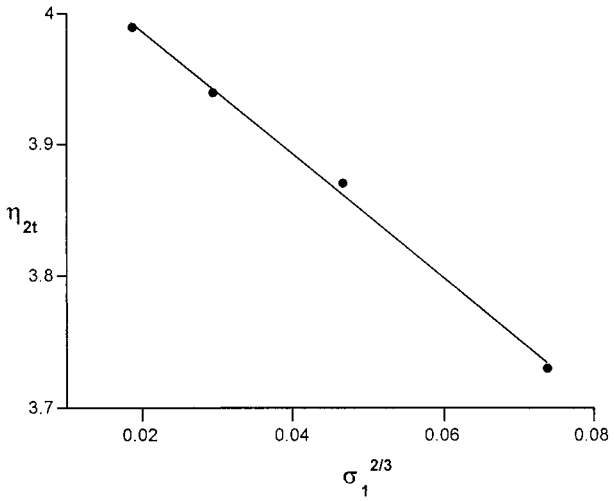

Figure 13. Position of the second transition point η_{2t} plotted vs $\sigma_1^{2/3}$according to eq 23; the data points were obtained by the SCF modeling for $N_1 = 800$ and $N_2 = 200$, at fixed $\sigma = 0.1$.

when the total thickness of the phase-segregated brush at the transition point is dominated by the outer CB layer:

$$\frac{d\rho}{d\eta} = \frac{d\rho}{dH}\frac{dH}{dM}\frac{dM}{d\mu_{LC}}\frac{d\mu_{LC}}{d\eta} \approx \text{const}\left(1 + \frac{N_2\sigma_2}{N_1\sigma_1}\right) \qquad (25)$$

For comparable grafting densities and $N_1 \gg N_2$ the slope becomes practically independent of the brush parameters, which is consistent with the results of the SCF computer modeling (see Figure 10).

The Onset of the One-Stage LC Ordering Mechanism. Now we can formulate the condition that determines when the two-stage ordering mechanism is replaced by the mixed one-stage mechanism. This happens when the second transition coincides with the first one. Equation 23 defines the second transition, while the first one is determined by eq 14 for in the reference monodisperse (N_2, σ) brush: $\tilde{\mu}_{LC} + \Delta\mu_t(N_2) = \mu_2$.

We have noted earlier that the first transition is exactly the same as in (N_2, σ) brush, so both μ_2 and the nucleation shift in the critical value of the LC phase chemical potential $\Delta\mu_t(\sigma,N_2) = \mu_t(\sigma,N_2) - \mu_t(\sigma,\infty)$ are to be taken at the original composition $\sigma = (\sigma_1 + \sigma_2)$. Combining these equations, one arrives at

$$\Delta\mu_t(N_2) = \frac{3}{2}\left(\frac{\pi\nu}{2}\right)^{2/3}\sigma^{2/3}(1 - (\sigma_1/\sigma)^{2/3}) \qquad (26)$$

The shift in μ_t is linearly related to the shift in η_t. It follows that eq 26 defines the position of the break points on the curves η_t vs (σ_2/σ) of Figure 12. Since $\Delta\eta_t(N_2)$ is typically much less than 1, eq 26 is well approximated by

$$\sigma_2^*/\sigma \cong \text{const}\cdot\sigma^{-2/3}\Delta\eta_t(N_2) \qquad (27)$$

It follows clearly that the position of the break point does not depend on N_1, in agreement with Figure 12.

The prediction of eq 27 is verified in Figure 14 where the break point values σ_2^*/σ extracted from the SCF modeling results for bidisperse brushes are plotted against $\eta_t(N_2)$ obtained for monodisperse brushes. We conclude that our analytical theory provides a uniform

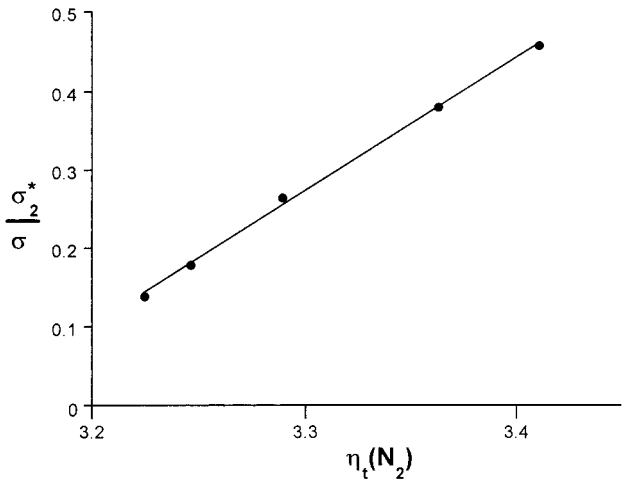

Figure 14. Break-point values of the relative fraction of short chains, σ_2^*/σ, determining the onset of the one-stage ordering in a bidisperse brush, vs the transition point in the reference monodisperse (N_2, σ) brush. The data points are obtained for $N_1 = 800$, $\sigma = 0.1$; $N_2 = 100$, 125, 200, 300, 400. The analytical theory predicts a linear dependence.

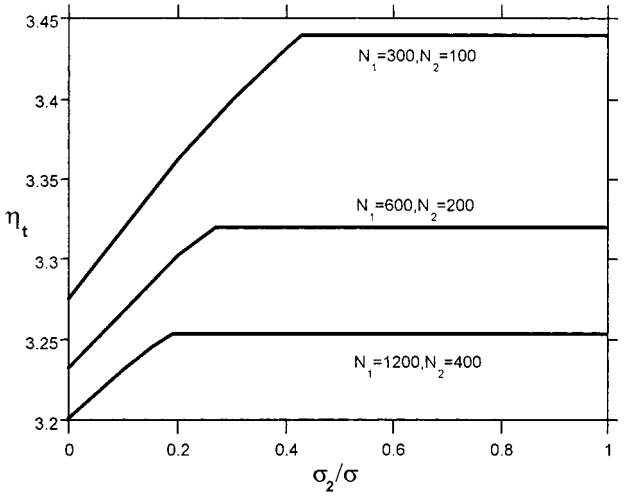

Figure 15. Chain length effects on the transition point curves η_t vs σ_2/σ at fixed N_2/N_1 ratio. The domain of the mixed one-stage mechanism shrinks as N_2 increases. N_1 and N_2 are indicated in the figure; $\sigma = 0.1$.

picture linking together the results of numerical modeling of various brush systems.

If one plots the curves η_t vs (σ_2/σ) for increasing values of N_2 while keeping the same value of σ, the position of the break point shifts to zero linearly with $\Delta\eta_t(N_2)$. When the ratio $q = N_2/N_1 < 1$ is fixed, the difference between the ordinates at the break point and at zero also decreases, as seen in Figure 15. The whole effect eventually vanishes in the $N_2 \to \infty$ limit. It is curious to note that the slope remains essentially the same for any large but finite N_2.

It is obvious from the reasoning given above that once the fraction of shorter chains (σ_2/σ) in the original composition falls below the value determined by eq 27, the LC ordering should go via the mixed one-stage mechanism. All the shorter chains and some of the longer chains are incorporated in the critical nucleus at the transition point. The transition value η_t is between the respective values for monodisperse (N_1, σ) and (N_2, σ) brushes. With further increase in η the remaining longer chains gradually join the LC sublayer.

IV. Discussion

The proposed framework for understanding the extended phase coexistence and related effects (the N-dependence of the critical nucleus size and the shifts in the transition point values) is applicable whenever the Gibbs free energy of a phase-segregated state is a convex-down function of the phase composition. Of course, it is well understood by now that only certain types of attractive interactions can result in collapse transitions in brushes. However, once the fact of phase coexistence is established, the exact nature of interactions that bring about its very possibility becomes irrelevant to the questions we discuss. Hence, we expect the proposed theoretical framework to have a very broad applicability.

Polyelectrolyte Brushes. Phase transitions and microphase coexistence were found in polyelectrolyte brushes under conditions of low salt concentration (the osmotic brush regime) by SCF computer modeling.[15−17] Some of the results were presented above in section 2. Qualitatively, the effects are similar to those discussed above for the LC brushes and can be traced to the form of the Gibbs free energy curve as a function of the phase composition.

Again, the collapsed phase is "normal" in the sense that the chemical potential is independent of the number of particles in it. The free energy of the swollen phase (per unit area) consists of the elastic contribution $\sigma H^2/N$ and the translational entropy of the counterions $H\alpha\rho \ln(\alpha\rho)$, where H is the brush height, $\rho = N\sigma/H$ is the segment density inside the brush, and α is the degree of ionization (assumed to be constant). In the osmotic brush regime, $\rho = \sigma\alpha^{-1/2}$ and $H = \alpha^{1/2}N$, so that the total free energy can be rewritten in the following form:

$$G = (A\sigma + B\sigma \ln \sigma)N \tag{28}$$

where A and B are certain constants. The second term ensures that the second derivative of the free energy $1/N^2\ \partial^2 G/\partial\sigma^2 \sim (N\sigma)^{-1}$ is positive. Hence, the analytical theory we presented above (with necessary modifications) is applicable.

It is worth noting that the first-order transition effects in PE brushes are observed only under condition of very small grafting density, $\sigma < \sigma_{cr}$ where $\sigma_{cr} \approx 1/80$ is the critical grafting density (the limiting point of the first order phase transition surface in the parameter space). For comparison, the critical grafting density in LC brushes is approximately 1 order of magnitude higher, $\sigma_{cr} \approx {}^1/_5$.

de Gennes *n*-Cluster Model. Brushes composed of chains with isotropic segment−segment interaction characterized by anomalous behavior of higher virial coefficients were shown to exhibit the collapse transition and microphase coexistence.[19] It was noted that there is a fundamental similarity between PE brushes and brushes with n-cluster attraction: in both cases the higher virial term changes sign while the dominant low-density term still remains positive. It is this competition that causes the brush to start collapsing in a discontinuous way. For a PE brush with standard isotropic attraction, the first-order virial term remains positive while the second virial coefficient changes sign. In the n-cluster model, it is the second virial term that remains positive while the nth coefficient ($n \geq 3$) changes sign.

Obviously, the low-density swollen brush phase in the *n*-cluster model is analogous to the CB phase discussed above, and the collapsed phase is expected to be "normal" since it is little affected by the effects of chain stretching. We conclude that all the effects discussed for LC brushes should apply (at least qualitatively) to microphase coexistence in brushes with *n*-cluster interactions.

V. Conclusion

Polymeric brushes with anisotropic attraction and polyelectrolyte brushes exhibit unusual microphase coexistence which takes place in a wide range of temperatures (at fixed zero external osmotic pressure). We present an analytical theory that serves as a basis for understanding this phenomenon. The key observation is that the exchange chemical potential of the swollen brush microphase changes is a function of the phase size. Hence, in contrast to common fluids, coexistence is not restricted to a line in the $P-T$ plane. Starting with the case of monodisperse brushes, the theory clarifies the nature of the first-order transition initiating the ordering. We predict the effect of the chain length, N, on the transition point and on the size of the critical nucleus of the ordered phase, in agreement with the results of SCF computer modeling.

The framework of the theory can be extended to the case of bidisperse brushes composed of chains of two fractions differing in contour length. Here, we are able to explain two mechanisms of ordering observed in the SCF computer modeling. Predictions for certain important features of the ordering (character of transitions, shifts of the transition points, and parameter domains of ordering mechanisms) are found in good agreement with the results of SCF computer modeling.

We expect the framework of the proposed phenomenological theory of extended phase coexistence to be of a broad applicability.

Acknowledgment. We acknowledge the Russian Foundation for Basic Research (Grant 99-03-33319), INTAS (Grant 99-01852), and NWO Dutch-Russian program (Polyelectrolytes in Complex Fluids) for financial support. L.K. is grateful to the Center for Advanced Mathematical Sciences at the American University of Beirut for letting use its facilities.

References and Notes

(1) Borisov, O. V.; Zhulina, E. B.; Birshtein, T. M. *Polym. Sci. USSR* **1988**, *30*, 772.
(2) Halperin, A. *J. Phys. (Paris)* **1988**, *49*, 547.
(3) Zhulina, E. B.; Borisov, O. V.; Pryamitsyn, V. A.; Birshtein, T. M. *Macromolecules* **1991**, *24*, 140.
(4) Borisov, O. V.; Birshtein, T. M.; Zhulina, E. B. *J. Phys. II* **1991**, *1*, 521.
(5) Pincus, P. *Macromolecules* **1991**, *24*, 2912. Ross, R. S.; Pincus, P. *Macromolecules* **1992**, *25*, 2177.
(6) Birshtein, T. M.; Borisov, O. V.; Mercurieva, A. A.; Zhulina, E. B. *Prog. Colloid Polym. Sci.* **1991**, *85*, 38.
(7) Zhulina, E. B.; Borisov, O. V.; Birshtein, T. M. *J. Phys. II* **1992**, *2*, 63.
(8) Ross, R. S.; Pincus, P. *Europhys. Lett.* **1992**, *19*, 79.
(9) Pickett, G. T.; Witten, T. A. *Macromolecules* **1992**, *25*, 4569.
(10) Birshtein, T. M.; Mercurieva, A. A.; Pryamitsyn, V. A.; Polotsky, A. A. *Macromol. Theory Simul.* **1996**, *5*, 215.
(11) Birshtein, T. M.; Mercurieva, A. A.; Klushin, L. I.; Polotsky, A. A. *Comput. Theor. Polym. Sci.* **1998**, *8*, 179.
(12) Klushin, L. I.; Birshtein, T. M.; Mercurieva, A. A. *Macromol. Theory Simul.* **1998**, *7*, 483.
(13) Amoskov, V. M.; Birshtein, T. M.; Pryamitsyn, V. A. *Macromolecules* **1996**, *29*, 7240.
(14) Birshtein, T. M.; Amoskov, V. M.; Mercurieva, A. A.; Pryamitsyn, V. A. *Macromol. Symp.* **1997**, *113*, 151.
(15) Misra, S.; Mattice, W.; Napper, D. *Macromolecules* **1994**, *27*, 7090.
(16) Pryamitsyn, V. A.; Leermakers, F. A. M.; Fleer, G. J.; Zhulina, E. B. *Macromolecules* **1996**, *29*, 8260.
(17) Birshtein, T. M.; Amoskov, V. M. *Polym. Sci, Ser. C* **2000**, *42*, 172.
(18) de Gennes, P. G. *C. R. Acad. Sci. Paris II* **1991**, *313*, 1117.
(19) Wagner, M.; Brochard-Wyart, F.; Hervet, H.; de Gennes, P. G. *Colloid Polym. Sci.* **1993**, *271*, 621.
(20) Amoskov, V. M.; Birshtein, T. M. *Macromolecules* **2001**, *34*, 5331.
(21) de Gennes, P. G. *J. Chem. Phys.* **1974**, *60*, 5030.
(22) Zhulina, E. B.; Borisov, O. V.; Priamitsyn, V. A. *Polym. Sci. USSR* **1989**, *31*, 185.
(23) Milner, S. T.; Witten, T. A.; Cates, M. E. *Macromolecules* **1988**, *21*, 2610.
(24) Birshtein, T. M.; Lyatskaya, Yu. V.; Zhulina, E. B. *Polymer* **1990**, *31*, 2185.
(25) Milner, S. T.; Witten, T. A.; Cates, M. E. *Macromolecules* **1989**, *22*, 853.

MA0105338